FINAL REPORT

Award Number: 01HQGR0012

# COMPARISON OF SEISMIC AND GEODETIC SCALAR MOMENT RATES ACROSS THE BASIN AND RANGE PROVINCE

Element II: Evaluate Urban Hazard and Risk

Aasha Pancha, John G. Anderson
Seismological Laboratory and Department of Geological Sciences
Mail Stop 174
University of Nevada
Reno, Nevada, 89557.
Phone: 775-784-4975
Fax: 775-784-4165
Email: pancha@seismo.unr.edu, jga@unr.edu

Principal Investigator: John G. Anderson

Research supported by the U. S. Geological Survey (USGS), Department of Interior, under USGS award number 01HQGR0012. The views and conclusions contained in this document are those of the authors and should not be interpreted as necessarily representing the official policies, either expressed or implied, of the U. S. Government.

Award Number: 01HQGR0012

# COMPARISON OF SEISMIC AND GEODETIC SCALAR MOMENT RATES ACROSS THE BASIN AND RANGE PROVINCE

Aasha Pancha, John G. Anderson
Seismological Laboratory and Department of Geological Sciences
Mail Stop 174
University of Nevada
Reno, Nevada, 89557.
Phone: 775-784-4975
Fax: 775-784-4165
Email: pancha@seismo.unr.edu, jga@unr.edu

## TECHNICAL ABSTRACT

Scalar moment rates estimated from a 146-year seismicity catalog agree, within uncertainties, with the deformation rate of the Basin and Range province determined using space geodesy. Seismic moment rates have been estimated from a new catalog of earthquakes intended to be complete for $M \geq 5$. The catalog was compiled from 15 preexisting catalogs, supplemented by the review of 42 published journal articles. Throughout the catalog compilation, care was taken to obtain the moment magnitude or a reasonable, and not inflated, equivalent. 80% of the moment release occurred during 10 earthquakes of magnitude $M_W \geq 6.79$. The spatial pattern of earthquakes matches the geodetic pattern of deformation. About 75% of the seismic moment release, and 70% of the geodetic deformation, takes place in a 200 km zone along the western edge of the province, matching the pattern of the cumulative earthquake numbers. Several techniques, ultimately traceable to Kostrov and Brune, are used to translate the geodetic strain rates into rates of seismic moment release. Rates determined from seismicity, of $4.5\times10^{25}$ to $10.8\times10^{25}$ dyne-cm/year, overlap the range determined from the geodetic data, $5.87\times10^{25}$ to $13.0\times10^{25}$ dyne-cm/year. This agreement suggests that within uncertainties, the rate of historic earthquakes within the Basin and Range province, taken as a whole, provides a reasonable estimate for the future rate of seismicity. These results support the hypothesis that even a few years of detailed geodetic monitoring can provide a good constraint on seismic hazard estimates.

## Non-Technical Abstract

Rates deformation release estimated from a 146-year seismicity catalog agree, within uncertainties, with new data on the deformation rate of the Basin and Range province determined using space geodesy. The spatial distribution of earthquakes and their moment release matches the geodetic pattern of deformation. All three are concentrated in a ~ 200 km zone along the western boundary which widens to the north. These results support the hypothesis that even a few years of detailed geodetic monitoring can provide a good constraint on seismic hazard estimates.

**Introduction:**
Earthquake occurrence rates are essential for seismic hazard analysis. The adequacy of seismic catalogues for seismic hazard analysis is governed by the product of the area of interest, catalogue duration (Smith, 1976), and regional strain rate (Ward, 1998a); the catalog duration is almost always insufficient. Fault slip rates and crustal deformation rates may be used to compensate for inadequate catalogs. Geological data on fault slip rates are labor intensive and difficult to obtain, as the appropriate fault exposures are often not available. Geodetic data on crustal deformation rates, in contrast, are relatively easily obtained with just a few years of observations using the Global Positioning System (GPS). It seems reasonable that these contemporary strain rates should also correlate with earthquake rates (e.g. Shen-Tu *et al*, 1998; Ward, 1998a; Ward, 1998b; Shen-Tu *et al*, 1999) but the hypothesis has not been widely tested. The Basin and Range province extends from the rigid Sierra Nevada block in the west to the Colorado Plateau in the east (Figure 1). The province is an actively deforming region of Cenozoic extension, characterized by north trending ranges, of relatively uniform spacing and elevation, which are bounded by normal faults and separated by basins. Early extension may be related to buoyancy forces within the lithosphere (Wernicke, 1992), while present day extension may be related to high gravitational potential energy of the elevated Western United States moderated by forces exerted by bounding plates and low-density magmatic contributions to the lithosphere (Lachenbruch & Morgan, 1990; Jones *et al*, 1996; Humphreys, 1998, Thatcher *et al*, 1999).

The orientation of the normal faults within the Basin and Range is consistent with the orientation of stresses needed to produce right lateral slip along the San Andreas Fault system. Portion of the Pacific–North American relative plate motion is taken up by displacement and deformation in the Basin and Range province, with relative motion between the Sierra Nevada – Great Valley microplate and the central Great Basin , indistinguishable from the Pacific – North American plate motion (Bennett *et al*, 2003). Motion west of about 118 W are in agreement with Pacific Plate motion (Thatcher 1999; Hammond and Thatcher, in press), suggesting coupling of the plate motion.

Geodetic measurements show concentrated deformation at the eastern (~50 km) and western (~200 km) edges of the region, coinciding with regions of modern seismicity, with little deformation between (Thatcher *et al*, 1999; Bennett *et al*, 2003; Hammond and Thatcher, in press). The style of Basin and Range deformation varies across six tectonic domains delimited by strain transitions. The greatest deformation takes place across a zone of conjugate strike-slip and normal faults, at a rate of 12.5 ± 0.15 mm/year between 119.1°W and 120.2°W. More recent data confirm this observation, with velocities west of 117.7°W increasing from ~1 mm/yr to ~12 mm/yr (Hammond and Thatcher, in press; Bennett *et al*, 2003). Strain rates increase from north to south along this western boundary of the region (Bennett *et al*, 2003). These high velocity gradients imply high seismic risk, increasing the potential for more frequent damaging earthquakes.

We studied the relationship between the spatial pattern of seismicity and geodetic strain in the Basin and Range province. We also compare the historical earthquake occurrence rates with those inferred from geodetic strain rates. The rate comparison is quantified as a comparison of

seismic moment rates, as seismic moment is related to both the amount of deformation and the consequent character of ground motions measured on seismograms.

**Analysis and Results:**

The study area is outlined in Figure 1. The southwestern boundary of the study area (Figure 1) runs down the crest of the rigid Sierra Nevada Range, California, and extends on the same trend to include regions in the Mojave Desert where deformation is more related to the northward motion of the Sierra Nevada mountains than to the main motion of the San Andreas fault. Seismic moment rates have been estimated from a new catalog of earthquakes intended to be complete for magnitude $M \geq 5$ (Figure 1). Earthquakes within the study region with $M \geq 4.8$ in any of 15 preexisting catalogs were supplemented by the results of 37 journal articles. The final catalog has 800 earthquakes, and 487 earthquakes with $M \geq 5.0$ since 1855. Several of the catalogs and individual studies include an earthquake in 1852 in western Nevada, with M=7.3. The anecdotal evidence is not sufficient to assign a magnitude and location that is reliable enough for this study.

For most earthquakes, seismic moment is estimated from magnitude. Moment magnitude ($M_W$) estimates were selected when available. For the most significant events, where many $M_W$ estimates were available, criteria were followed to select the most favored $M_W$ value. The Harvard long period surface wave estimates of the seismic moment have been consistent for the last 33 years and hence were given primary preference. Other surface wave estimates, followed by body wave, geological and geodetic estimates were then considered. For the other earthquakes, care was taken avoid inflated magnitude estimates, usually by using the smallest magnitude from any catalog. This yields a lower-bound estimate for the occurrence rate of moderate-sized earthquakes.

The magnitudes were then treated as moment magnitude. The seismic moment of each event was estimated using the relation (Hanks and Kanamori, 1978)

$$M_o = 10^{\frac{3}{2}M_W + 16.05} \quad .$$

We have confirmed this relation for moderate-magnitude earthquakes in Nevada. Considering completeness intervals for various magnitudes, the discrete Gutenberg-Richter relation for the number of earthquakes, *n*, equal to magnitude $M \pm 0.5$ is $\log n = 5.83 - 1.01M$. Using cumulative rates of occurrence over appropriate catalog durations, a relation of $\log N = 6.27 - 1.09M$ was obtained, predicting 4.4 earthquakes per century with $M_W \geq 7.0$, 0.53 earthquakes per year with $M_W \geq 6.0$, and 6.6 earthquakes per year with $M_W \geq 5.0$. The *b*-value for either relationship is typical. Of the total moment, 80% was released during 10 earthquakes of magnitude $M_W \geq 6.79$, and 90% was released in the 29 events of $M_W \geq 6.3$. Thus small events do not significantly release the accumulating strain.

Figures 2.1, 2.2 and 2.3 show the spatial distribution of earthquake numbers, of moment release, and of crustal deformation as a function of perpendicular distance from the southwestern boundary of the study region. Three domains, each 300 km wide as illustrated in Figure 1, are shown, a southern (~35N°), a central (~37N°) and a northern zone (~40N°). The geodetic profile

utilizes averaged geodetic rates obtained from geodetic, Satellite Laser Ranging and Very Long Baseline Interferometry data obtained across the Basin and Range from more than 42 studies (Kreemer et al, 2000, 2003, personal communication). Deformation is concentrated within a zone of about 200 km width along the southwestern edge of the province, coinciding with the Northern Walker Lane (Stewart, 1988). The plots show that the spatial patterns of seismic activity, seismic moment, and geodetic deformation are similar along all of the profiles. They all clearly show a northward widening of the deformation zone along the western edge of the province. Within the southern domain (Figure 2.1), deformation is concentrated within a 50 km zone, accommodating about 60% of the geodetic deformation, 60% of the seismic moment rate and 70% of the earthquakes. Across the central domain, the earthquake count and geodetic deformation follow the same trend with 85% of the earthquakes and 85% to 95% of the geodetic deformation occurring within a 200 km zone. This is in contrast to the seismic moment rate, 95% of which is released within 30 km of the western edge, the moment release begin dominated by the 1872 Owens Valley event (Table 2), the largest event in the catalog. The greatest deformation rate evident from the geodetic data occurs across a 100 km zone. The northern domain has 90% of its earthquakes, 60% of the moment release, and 70% to 90% of the geodetic deformation occurring across a 200km zone. Deformation is dominated by the 1954 seismic activity, which includes four of the largest events in the region, and the Cedar Mountain event (Table 2), along with associated aftershocks.

Figure 2.4 shows that activity along the eastern half of the Great Basin is significantly smaller than in the west. The greatest increase on all three rates in Figure 2.4 occurs at the very eastern edge of the Basin and Range. About 25% of the earthquakes and 18% of the seismic moment are concentrated east of 113°W. Less than about 8% of the deformation measured with GPS occurs there.

Some uncertainties affect Figure 2. The earthquake count lacks aftershocks of the 1872 (southwestern domain) and 1915 (northwestern domain) earthquakes, the 1872 earthquake being the largest in the catalog. If those aftershocks were included the earthquake rate might also become as concentrated as the seismic moment in the western part of the profile. In general, all curves within the scatter of the data, the spatial patterns of seismic activity, seismic moment, and geodetic deformation are the same.

The historical seismic moment rate is estimated from Figure 3a using a statistical approach. The seismic moment is a tensor. Here the magnitude of the maximum eigenvalue is used. Although tensor information is available for the ten largest earthquakes, which release 80% of the total seismic moment, use of tensors increases the number of degrees of freedom, and therefore requires a longer observation time to obtain a reliable comparison. A fit to the end points of the cumulative rate curve with time gives an average rate of $9.02 \times 10^{25}$ dyne-cm/year. Figure 3a shows a non-unique but plausible rationale for moment rates as low as $6.05 \times 10^{25}$, or as high as $10.06 \times 10^{25}$ dyne-cm/year. A least-squares fit to the points in Figure 3a (1 point for each year with an earthquake) has a slope of $7.28 \pm 0.5 \times 10^{25}$ dyne-cm/yr. Note that the lower bound on the cumulative moment corresponds to the upper bound on the moment rate estimate from historical earthquakes. To quantify and assess uncertainties associated with these seismic moment rates, the procedure shown in Figure 3a was repeated, using (1) instead upper-bound estimates of the smaller events and (2) Monte Carlo realizations.

Earthquake magnitude selection was repeated for the smaller events without $M_W$ estimates, with the largest magnitude of any listed catalog being selected as the favored magnitude instead of the smallest. This yields a catalog representing an upper bound estimates for the occurrence rate. Figure 3b shows the results of use of this upper bound catalog. A fit to the end points of the cumulative rate curve gives an average rate of $10.07 \times 10^{25}$ dyne-cm/year. Figure 3b shows moment rates as low as $6.56 \times 10^{25}$, or as high as $10.83 \times 10^{25}$ dyne-cm/year, while least-squares fit to the points give a slope of $7.93 \pm 0.5 \times 10^{25}$ dyne-cm/yr.

The procedure in Figure 3a was also automated and repeated for randomly chosen moments of the ten largest earthquakes, which control the total moment release. Moment release for each of these events was randomly selected assuming a constant probability density between minimum and maximum $M_W$ estimates. The maximum and minimum $M_W$ values were selected based on the most reliable and appropriate estimates of $M_W$ from the literature (Table 2). Moment release for all other earthquakes was held constant at the favored values based on lower bound estimates. Data points corresponding to those used to calculate rates by eye were applied. A total of 50,000 Monte Carlo realizations were generated. From these realizations, distribution of the minimum, average, and maximum rates are shown in Figure 4 and summarized in Table 3 along with results from Figure 3. A least-squares fit to each realization was also calculated. Considering one standard deviation about the mean values, the moment rate ranges from 5.07E+25 to 8.67E+25 dyne-cm/yr. Extremes selected by the visual approach (Figure 3) are outside the two-standard-deviation limits of the least squares fit. The absolute range of moment rates determined via the Monte Carlo method range from 4.17E+25 to 10.09E+25 dyne-cm/year. Thus limits on the moment rate from historical seismicity are $4.2 \times 10^{25}$ to $10.8 \times 10^{25}$ dyne-cm/year.

The range of moment rates, determined above, can be compared with moment rates that can be estimated from the geodetic deformation rates. To do this we need models that relate the deformation rates to moment rates. Methods to estimate moment rates from the crustal deformation rates are available in the literature, assuming all deformation occurs seismically. For a fault with average geological slip rate $\dot{s}$, the moment rate is predicted to be

$$\dot{M}_o = \mu A \dot{s} \qquad (1)$$

where μ is the shear modulus, and $A$ is the total area of fault that ruptures seismogenically (Brune, 1968). As this equation is independent of the width of the zone, it can be extended for a volume subjected to a uniform stress field, in which all faults are parallel to the margin. Where crustal deformation is expressed as a broad zone of deformation, with numerous faults of variable orientation and importance, it is appropriate to use regional strain rates instead of the slip rate. Techniques have been proposed to translate the tensor geodetic strain rate into rates of scalar seismic moment release. Kostrov (1974) and Ward (1998a) relate the average strain rate over a volume and the sum of earthquake moment tensors. The moment rate is reduced to a scalar quantity by replacing the tensor strain rate by its largest eigenvalue and the tensor moment rate by a scalar quantity. An assumption is made that the average surface strain is representative of the volume strain at depth. Methods to estimate moment rates from the crustal strain rates are available in the literature, however, there is variation in the literature over the best scalar representation of surficial strain.

Anderson (1979) modeled a volume extending or contracting in one direction, (say $x_2$), presenting a best estimate solution to the problem as

$$\dot{M}_o = 2\mu L_1 L_2 W \dot{\varepsilon}_2 / k \quad (2)$$

where $L_1$ is the length of the region, $L_2$ is the width of the region in the direction that it is straining, *W* is the seismogenic thickness, and $\dot{\varepsilon}_2$ is the strain rate. The strain rate in turn is given by $\dot{\varepsilon}_2 = V_2 / L_2$ where $V_2$ is the relative extension or convergence velocity of the opposite sides of the region. Parameter *k* is a dimensionless constant that adjusts for the inefficiency of randomly oriented faults to accommodate strain.

Ward (1994, 1998a,b) proposes a minimum rate which incorporates the maximum eigenvalue i.e. the principle surficial extension and contraction rates with

$$\dot{M}_o = 2\mu W \Sigma Max\left(|\dot{\varepsilon}_1|, |\dot{\varepsilon}_2|\right) \quad (3).$$

where $\dot{\varepsilon}_1$ and $\dot{\varepsilon}_2$ are the principle surficial extension and contraction rates, and $\Sigma$ is the surface area of the region. The Working Group on California Earthquake Probabilities (1995) also uses a minimal approach to represent the moment rate tensor, utilizing the difference between the principal strain rates

$$\dot{M}_o = 2\mu W \Sigma\left(\dot{\varepsilon}_1 - \dot{\varepsilon}_2\right) \quad (4).$$

Correspondence of the scalar moment rate with a given surface strain accumulation is non-unique. Savage and Simpson (1997) emphasize that the moment tenor is resolved into the superposition of two or more double-couple mechanisms, and this resolution can be done in many ways. Savage and Simpson (1997) therefore suggest the preferred estimate is that which produces the smallest scalar moment rate, equivalent to the principal surface strain rates acting over a region, given by:

$$\dot{M}_o^{(\min)} = 2\mu W \Sigma Max\left(|\dot{\varepsilon}_1|, |\dot{\varepsilon}_2|, |\dot{\varepsilon}_1 + \dot{\varepsilon}_2|\right) \quad (5)$$

Recognizing the area $\Sigma$ in Eqs (3), (4) and (5) to be equivalent to $L_1 L_2$ in Eq (2), these equations are similar. Eq. (5) accommodates strain in multiple directions but if strain is only in the $x_2$ direction the strain rate terms are identical. Eq (2) converges to Eq. (5) when *k*=1. Savage and Simpson noting that their method gives similar results to Ward and only differs if $\dot{\varepsilon}_1$ and $\dot{\varepsilon}_2$ have the same sign, while the Working Group representation is much less.

Acknowledging the non-uniqueness and uncertainty involved with converting surface strain to a scalar moment rate, this study utilizes all four methods discussed above to help quantify the moment rate from geodesy and its associated errors. We take the shear modulus to be $\mu=3\text{x}10^{11}$ dyne/cm$^2$ (Anderson, 1979) and assume all deformation occurs seismically above a brittle-ductile transition depth of *W*=15 km, determined from the depth distribution of earthquakes. For a particular assumption about a random distribution of fault orientation, Anderson (1979) found *k*=0.64, probably giving a lower limit to this parameter. Total scalar moment and deformation rates for central Asia and southern California are consistent with *k*=0.75 (Anderson, 1979; Chen and Molnar, 1979), and this value is therefore applied in this study.

We predict the moment rate for the Basin and Range province from geodetic, Satellite Laser Ranging and Very Long Baseline Interferometry data obtained across the Basin and Range from

more than 42 studies and inverted for strain rate tensor components (Kreemer et al, 2000, 2003, personal communication). Whilst the bi-cubic Bessel interpolation of the data smoothes the data to a degree, additional smoothing is applied to account for the distribution of geodetic data. Both the unsmoothed data (underdamped, and smoothed data (damped) data are used in separated calculations to estimate the moment release from the geodetic deformation rates. The results are summarized in Table 4. Resulting moments from geodesy are in the range from $5.87 \times 10^{25}$ to $21.41 \times 10^{25}$ dyne-cm/year.

Fault parameters used as input to the 1996 and 2002 USGS seismic hazard maps (Frankel et al, 1996, 2000) are utilized to determine the moment rate from geology from Eq (1). Data for California are taken from the 1996 model, while all other data for the study region are taken from the 2002 model. We assume $\mu=3 \times 10^{11}$ dyne/cm$^2$. Resultant geological moment rates for the region are much lower than both the seismicty and geodetic rates (Table 5, Figure 5). This is not surprising considering the limit paleoseismic data. Uncertainties associated with the measurement of the fault parameters, would reflect in uncertainties in the moment rate presented here. Although beyond the scope of this study, inclusion of these uncertainties may result in the geological moment rate being of the same order of magnitude as the seismicity rate.

Rates determined from seismicity, of $4.5 \times 10^{25}$ to $10.8 \times 10^{25}$ dyne-cm/year, substantially overlap the range determined from the geodetic data, $5.87 \times 10^{25}$ to $21.41 \times 10^{25}$dyne-cm/year (Figure 5). This suggests that the rate of historic earthquakes within the Basin and Range province, taken as a whole, is within a factor of two of the rate that should be expected in the future. Following from the suggestion of Smith (1976) and Ward (1998a), we define $Z = T\Sigma\bar{\dot{\varepsilon}}$, the product of the duration of the earthquake record ($T$), the area of the region, and the average strain rate, $\bar{\dot{\varepsilon}}$. For $T$=146 years, $\Sigma = 1.28 \times 10^6$ km$^2$, and $\bar{\dot{\varepsilon}} = 1.2 \times 10^{-8}$/yr, $Z \approx 2.2$ km$^2$. Based on these Basin and Range results, it is reasonable to expect that in other regions with $Z \geq 2$ km$^2$, historical seismicity and geodesy will agree within uncertainties of about a factor of two.

## Conclusions

The most important conclusion of this study is that the geodetic spatial distribution is consistent with the spatial distribution of the seismic moment release, and that the rate of earthquakes implied by geodesy is consistent with the historical estimate. Assuming this is confirmed elsewhere, this result has worldwide implications. The adequacy of seismic catalogs for seismic hazard analysis is governed by the product of the area of interest, catalog duration (Smith, 1976), and regional strain rate (Ward, 1998a); the catalog duration is almost always insufficient. Geological data on fault slip rates are quite difficult to obtain, as the appropriate fault exposures necessary to obtain slip rates and magnitudes of past earthquakes are often not available. Geodetic data, in contrast, are relatively easily obtained with just a few years of observations. With deformation rates from space geodesy, seismic hazard and recurrence estimates can become much more reliable on a global scale.

## Bibliography

Pancha A., and J. G. Anderson, Comparison of seismic and geodetic scalar moment rates across the Basin and Range province, *Bull. Seism. Soc. Am.*, in preparation.

**References:**


Anderson, J. G., Estimating the seismicity from geological structure for seismic-risk studies, *Bull. Seism. Soc. Am.*, *69*, 135-158, 1979.

Anderson, J. G, and J. N. Brune, Methodology for Using Precarious Rocks in Nevada to Test Seismic Hazard Models, *Bull. Seism. Soc. Am.*, *89*, 456-467, 1999.

Barker, M. R., and D. I. Doser, Joint Inversion of Regional and Teleseismic Earthquake Waveforms, *J. Geophys. Res*., *93*, 2,037-2,045, 1988.

Beanland, S., and M. M. Clarke, Late Quaternary history of the Owens Valley fault zone, eastern California and surface rupture associated with the 1872 earthquakes, *Abstracts with programs, Geological Society of America*, *25*, 7, 1993.

Bennett, R. A., Wernicke, B. P., Niemi, N. A., and M. Friedrich, Contemporary strain rates in the northern Basin and Range province from GPS data, *Tectonics, 22*, doi:10.1029/2001TC1355, 2003.

Brune, J. N., Seismic moment, seismicity, and slip rate along major fault zones, *J. Geophys. Res*, *73*, 777-784, 1968.

Chen, W.-P., and P. Molnar, Seismic Moments of major earthquakes and the average rate of slip in Central Asia, *J. Geophys. Res*., *82*, 2945-2969, 1977.

Doser, D. I., Source Parameters and Faulting Processes of the 1959 Hebgen Lake, Montana, Earthquake Sequence, *J. Geophys. Res*., *90*, 4537-4555, 1985.

Doser, D. I., Earthquake Processes in the Rainbow Mountain-Fairview Peak-Dixie Valley, Nevada, Region 1954-1959, *J. Geophys. Res*., *91*, 12,572-12,586, 1986.

Doser, D. I., Source Parameters of Earthquakes in the Nevada Seismic Zone, 1915-1943, *J. Geophys. Res*., *93*, 15,001-15,015, 1988.

Doser, D. I., and H. Kanamori, Long-Period Surface Waves of four Western United States Earthquakes Recorded by the Pasadena Strainmeter, *Bull. Seism. Soc. Am*., *77*, 236-243, 1987.

Doser, D. I., and R. B. Smith, Source Parameters of the 28 October 1983 Borah Peak, Idaho, Earthquake from Body Wave Analysis, *Bull. Seism. Soc. Am*., *75*, 1041-1051, 1985.

Doser, D. I., and R. B. Smith, An Assessment of Source Parameters of Earthquakes in the Cordillera of the Western United States, *Bull. Seism. Soc. Am*., *79*, 1383-1409, 1989.

Frankel, A., C. Mueller, T. Barnhard, D. Perkins, E. Leyendecker, N. Dickman, S. Hanson, and M. Hopper, National seismic-hazard maps: documentation June 1996, U.S. Geological Survey, Open-file Report 96-532, 110 pp, 1996.

Frankel, A. D.; Petersen, M. D.; Mueller, C. S.; Haller, K. M.; Wheeler, R. L.; Leyendecker, E. V.; Wesson, R. L.; Harmsen, S. C.; Cramer, C. H.; Perkins, D. M.; and K. S. Rukstales, Documentation for the 2002 Update of the National Seismic Hazard Maps: U.S. Geological Survey Open-File Report 02-420, 2002.

Hammond, W. C., and W. Thatcher (2004), Contemporary tectonic deformation of the Basin and Range province, western United States: 10 years of observation with the Global Positioning System, *J. Geophys. Res*., in press.

Hanks, T. C., and H. Kanamori, A Moment Magnitude Scale, *J. Geophys. Res*., *84*, 2348-2350, 1978.

Hanks, T. C., J. A. Hileman, and W. Thatcher, Seismic Moments of the Larger Earthquakes of the Southern California Region, *Geol. Soc. America Bull*., *86*, 1131-1139, 1975.

Humphreys, E. D., Processes of Ongoing Deformation in the Western United States, paper presented at the American Geophysical Union Fall Meeting, December, 1998.

Jones, C. H., Unruh, J. R., and L. J. Sonder, The role of gravitational potential energy in active deformation in the southwestern United States, *Nature*, *381*, 37-41, 1996.

Kostrov, V. V., Seismic moment and energy of earthquakes, and seismic flow of rock, *Earth Physics*, *1*, 23-40, 1974.

Kreemer, C., Haines, J., Holt, W. E., Blewitt, G. and D. Lavallee, On the determination of a global strain rate model, *Earth, Planets Space*, 52, 765-770, 2000.

Kreemer, C., Holt, W. E. and J.Haines, An integrated global model of present-day plate motions and plate boundary deformation, *Geophys. J. Int*., *154*, 8-34, 2003.

Lachenburch, A. H. and P. Morgan, Continental extension, magmatism and elevation: formal relations and rules of thumb, *Tectonophysics*, *174*, 39-62, 1990.

Mason, D. B., Earthquake Magnitude Potential of the Intermountain Seismic Belt, USA, from Surface-Parameter Scaling of Late Quaternary Faults, *Bull. Seism. Soc. Am*., *86*, 1487-1506, 1996.

Savage, J. C. and L. M. Hastie, A Dislocation Model for the Fairview Peak, Nevada, Earthquake, *Bull. Seism. Soc. Am.*, *59*, 1937-1948, 1969.

Savage, J. C., and R. W. Simpson, Surface Strain Accumulation and the Seismic Moment Tensor, *Bull. Seism. Soc. Am.*, *87*, 1345-1353, 1997.

Shen-Tu, B., Holt, W. E., and A. J. Haines, Contemporary Kinematics of the western United States determined from earthquake moment tensors, very long baseline interferometry, and GPS observations, *J. Geophys. Res.*, *103*, 18,087-18,117, 1998.

Shen-Tu, B., Holt, W. E., and A. J. Haines, Deformation kinematics in the western United States determined from Quaternary fault slip rates and geodetic data, *J. Geophys. Res.*, *104*, 28,927-28,955, 1999.

Sieh, K., *et al*, Near-field investigations of the Landers earthquake sequence, April to July 1992, *Science*, *260*, 171-176, 1993.

Smith, S. W., Determination of maximum earthquake magnitude, *Geophys. Res. Letters*, *3*, 351-354, 1976.

Stewart, J. H., Tectonics of the Walker Lane Belt, western Great Basin; Mesozoic and Cenozoic deformation in a shear zone, in *Metamorphism and crustal evolution of the Western United States*, edited by W. G. Ernst, *7*, 683-713, Prentice-Hall, Englewood Cliffs, New Jersey, 1988.

Thatcher, W., Foulger, G. R., Julian, B. R., Svarc, J., Quilty, E. and G. W. Bawden, Present-Day Deformation Across the Basin and Range Province, Western United States, *Science*, *283*, 1714-1718, 1999.

Ward, S. N., A multidisciplinary approach to seismic hazard in Southern California, *Bull. Seism. Soc. Am.*, *84*, 1293-1309, 1994.

Ward, S. N., On the consistency of earthquake moment rates, geological fault data, and space geodetic strain: the United States, *Geophys. J. Int.*, *134*, 172-186, 1998a.

Ward, S. N., On the consistency of earthquake moment rates, geological fault data, and space geodetic strain: Europe, *Geophys. J. Int.*, *135*, 1011-1018, 1998b.

Wells, D. L., and K. J. Coppersmith, New Empirical Relationships among Magnitude, Rupture Length, Rupture Width, Rupture Area, and Surface Displacement, *Bull. Seism. Soc. Am.*, *84*, 974-1002, 1994.

Wernicke, B., Cenozoic extensional tectonics of the U.S. Cordillera, in *The Cordilleran Orogen: Conterminous U.S.: The Geology of North America*, edited by Lipman, P. W., Burchfiel, B. C., and M. L. Zoback, *G-3*, 553-581, Geological Society of America, Boulder, CO, 1992.

Working Group on California Earthquake Probabilities, Seismic hazards in southern California: probable earthquakes, 1994-2024, *Bull. Seism. Soc. Am., 85*, 379-439, 1995.

**Table 1: Catalogs included in the compiled earthquake database.**

| Catalogs Searched | Abbreviation | Web Address |
|---|---|---|
| Historical and Preliminary data | PDE | http://wwwneic.cr.usgs.gov/neis/epic/epic.html |
| Significant Earthquakes Worldwide | NOAA | http://wwwneic.cr.usgs.gov/neis/epic/epic.html |
| Significant US Earthquakes | USHIS | http://wwwneic.cr.usgs.gov/neis/epic/epic.html |
| California | CDMG | http://wwwneic.cr.usgs.gov/neis/epic/epic.html |
| Canada | EPB | http://wwwneic.cr.usgs.gov/neis/epic/epic.html |
| Mexico, Central America, Caribbean | NGDC | http://wwwneic.cr.usgs.gov/neis/epic/epic.html |
| Eastern, Central and Mountain States | SRA | http://wwwneic.cr.usgs.gov/neis/epic/epic.html |
| Nevada Seismological Laboratory, University of Nevada, Reno | UNR1852 | www.seismo.unr.edu/Catalog/catalog-search.html |
| University of California, Berkeley | BK | http://quake.geo.berkeley.edu/ncedc/catalog-search.html |
| Council of the National Seismic System | CNSS | http://quake.geo.berkeley.edu/cnss-catalog.html |
| Pasadena | SCSN | www.scecdc.scec.org/catalogs.html |
| Northern California Earthquake Data Center | NCSN | http://quake.geo.berkeley.edu/cnss/catalog-search.html |
| Utah (regional and historic) | | www.quake.utah.edu/catalog/catalog.shtml |
| Yellowstone | | http://www.quake.utah.edu/catalog/ynp.shtml |
| Harvard | | http://www.seismology.harvard.edu/CMTsearch.html |

**Table 2: Ten largest events in the compiled catalog.**

| Year | Month | Day | Hour | Minute | Latitude | Longitude | Preferred Magnitude $M_W$ | Minimum Magnitude $M_W$ | Maximum Magnitude $M_W$ | Earthquake Name |
|---|---|---|---|---|---|---|---|---|---|---|
| 1872[1] | 3 | 26 | 10 | 30 | 36.70 | -118.10 | 7.74 | 7.44 | 7.74 | Owens Valley |
| 1915[2] | 10 | 3 | 6 | 53 | 40.50 | -117.50 | 7.18 | 6.82 | 7.18 | Pleasant Valley |
| 1932[3] | 12 | 21 | 6 | 10 | 38.80 | -117.98 | 7.10 | 6.80 | 7.10 | Cedar Mountain |
| 1954[4] | 8 | 24 | 5 | 51 | 39.60 | -118.50 | 6.76 | 6.27 | 6.76 | Stillwater |
| 1954[5] | 12 | 16 | 11 | 7 | 39.20 | -118.00 | 7.12 | 6.91 | 7.35 | Fairview Peak |
| 1954[6] | 12 | 16 | 11 | 11 | 39.67 | -117.90 | 6.92 | 6.60 | 7.15 | Dixie Valley |
| 1959[7] | 8 | 18 | 6 | 37 | 44.88 | -111.10 | 7.32 | 7.25 | 7.42 | Hebgen Lake |
| 1983[8] | 10 | 28 | 14 | 6 | 44.96 | -113.90 | 6.93 | 6.70 | 7.20 | Borah Peak |
| 1992[9] | 6 | 28 | 11 | 57 | 34.20 | -116.44 | 7.29 | 7.22 | 7.30 | Landers |
| 1999[10] | 10 | 16 | 9 | 46 | 34.59 | -116.27 | 7.12 | 7.10 | 7.12 | Hector Mine |

[1] The preferred and maximum magnitude is from Hanks et al (1975), the minimum is from Beanland and Clarke (1993).
[2] The preferred and maximum magnitude is from Wells and Coppersmith (1994), the minimum is from Doser (1988).
[3] The preferred and maximum magnitude is from Wells and Coppersmith (1994), the minimum is from Doser (1986) and Doser and Smith (1989).
[4] The preferred and maximum magnitude is from Mason (1996), the minimum is from Barker and Doser (1988).
[5] The preferred magnitude is from Doser and Smith (1989), the maximum and minimum are from Doser and Kanamori (1987) and Doser (1986) respectively.
[6] The preferred magnitude is from Doser and Kanamori (1987), the maximum and minimum are from Doser and Kanamori (1987) and Doser and Smith (1989) respectively.
[7] The preferred magnitude is from Doser and Smith (1989), the maximum is from Savage and Hastie (1969) and minimum is from Doser (1985) and from Doser and Smith (1989).
[8] The preferred magnitude is from Harvard, the maximum and minimum are from Mason (1996) and Doser and Smith (1985) respectively.
[9] The preferred magnitude is from Harvard, the maximum and minimum are from Seih *et al* (1993) and Wells and Coppersmith (1994) respectively.
[10] The preferred and maximum magnitude is from Harvard, the minimum is from UC Berkeley and the Council of the National Seismic System catalogs.

**Table 3: Statistical distribution of seismic moment rates determined from 5000 Monte Carlo simulations.**

| Seismic Moment Rate dyne-cm/year | Preferred | Upper Bound | Minimum | Maximum | Mean | Standard Deviation |
|---|---|---|---|---|---|---|
| **Visual Lower Bound** | 6.05e+25 | 6.56e+25 | 4.17e+25 | 6.64e+25 | 5.42e+25 | 0.35e+25 |
| **Visual Upper Bound** | 10.06e+25 | 10.83e+25 | 5.72e+25 | 10.09e+25 | 7.92e+25 | 0.75e+25 |
| **End Points** | 9.02+25 | 10.07e+25 | 5.16e+25 | 9.04e+25 | 7.11e+25 | 0.67e+25 |
| **Least Squares** | 7.28e+25 | 7.93e+25 | 4.45e+25 | 7.78e+25 | 6.15e+25 | 0.47e+25 |

**Table 4. Moment rates from Geodesy**

| Citation | Equation * | Moment Rate dyne-cm/yr | |
|---|---|---|---|
| | | **Damped** | **Underdamped** |
| **Anderson (1979)** | $\dot{M}_o = 2\mu L_1 L_2 W \dot{\varepsilon}_2 / k$ | 10.31 e+25 | 21.41 e+25 |
| **Ward (1994, 1998a,b)** | $\dot{M}_o = 2\mu W \Sigma Max(\lvert\dot{\varepsilon}_1\rvert, \lvert\dot{\varepsilon}_2\rvert)$ | 7.73 e+25 | 16.06 e+25 |
| **Working Group (1995)** | $\dot{M}_o = 2\mu W \Sigma(\dot{\varepsilon}_1 - \dot{\varepsilon}_2)$ | 5.87 e+25 | 11.47 e+25 |
| **Savage and Simpson (1997)** | $\dot{M}_o^{(\min)} = 2\mu W \Sigma Max(\lvert\dot{\varepsilon}_1\rvert, \lvert\dot{\varepsilon}_2\rvert, \lvert\dot{\varepsilon}_1 + \dot{\varepsilon}_2\rvert)$ | 7.89 e+25 | 16.55 e+25 |

* where $L_1$ is the length of the region, $L_2$ is the width of the region in the direction that it is straining, W is the seismogenic thickness, $\dot{\varepsilon}_2 = V_2 / L_2$ where $V_2$ is the relative extension or convergence velocity of the opposite sides of the region, $\dot{\varepsilon}_1$ and $\dot{\varepsilon}_2$ are the principle surficial extension and contraction rates, and $\Sigma$ is the surface area of the region, *k* is a dimensionless constant that adjusts for the inefficiency of randomly oriented faults to accommodate strain.

**Table 5: Comparison of moment rates for the Basin and Range province.**

| Data/Method* | | Moment Rate (dyne-cm/yr) |
|---|---|---|
| **1. Seismicity** | | 4.17 to 10.09 e+25 |
| **2. Geodesy** | | 5.87 to 21.41 e+25 |
| **3. Geology** | **USGS 2002/1996 data** $\dot{M}_o = \mu A\dot{s}$ | 2.54 e+25 |

***** Assuming $\mu=3x10^{11}$ dyne/cm$^2$ for geodesy and geology.

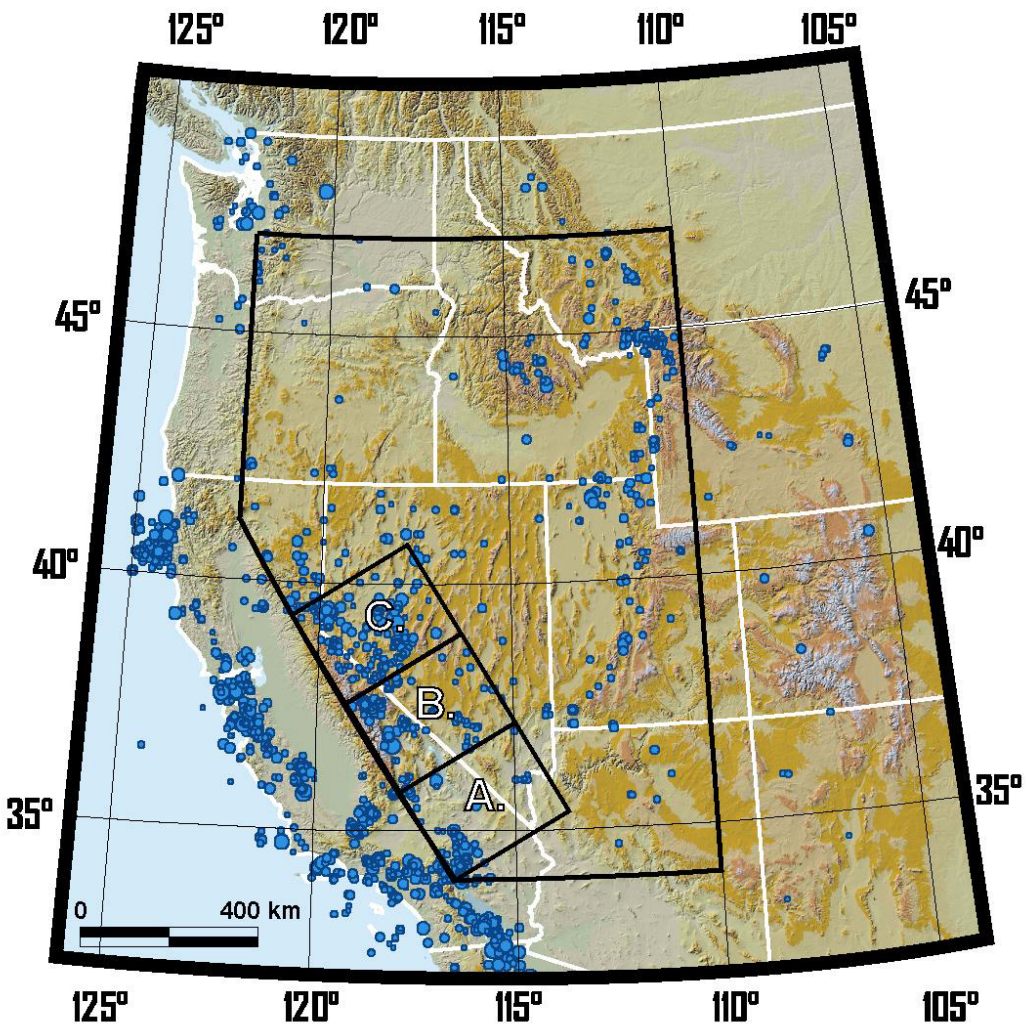


**Figure 1:** Map of the western United States, showing topography, earthquakes with M ≥ 4.8 (blue circles with radius proportional to magnitude). The study area, outlined with a bold polygon, encloses all major earthquakes that can be associated with deformation of the Basin and Range province. Regions A, B and C refer to the Southwestern, Central and Northwestern sub regions shown in Figure 2.

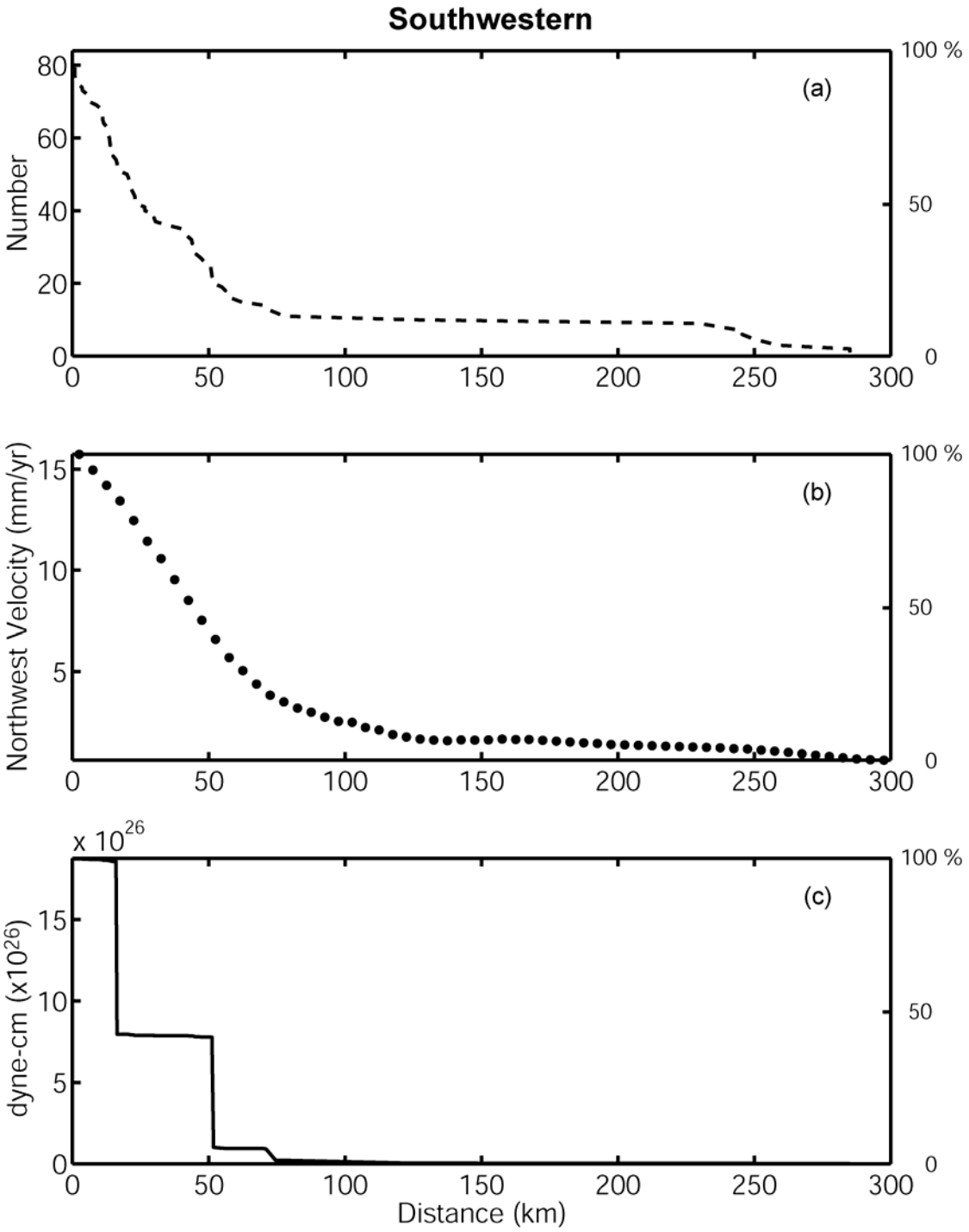


**Figure 2.1** Profiles through three domains, 300 km wide, along the western edge of the province are shown. (a) Cumulative number of earthquake events (b) averaged N37°W components of velocity determined from inversion of geodetic data (Kreemer, personal communication) and (c) cumulative seismic moment release, as a function of the perpendicular distance from the southwestern boundary of the study region (Figure 1).

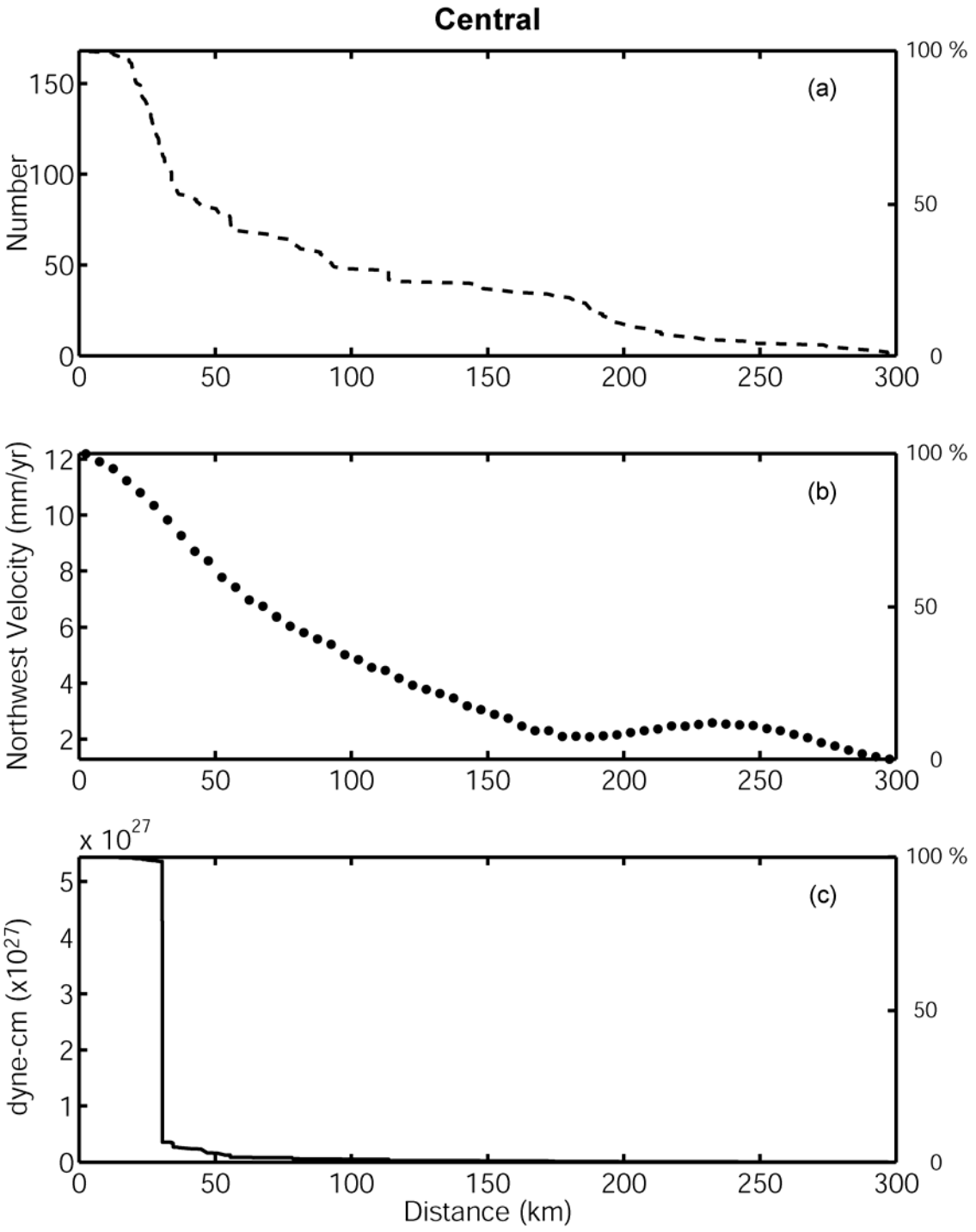


**Figure 2.2** Profiles through three domains, 300 km wide, along the western edge of the province are shown. (a) Cumulative number of earthquake events (b) averaged N37°W components of velocity determined from inversion of geodetic data (Kreemer, personal communication) and (c) cumulative seismic moment release, as a function of the perpendicular distance from the southwestern boundary of the study region (Figure 1).

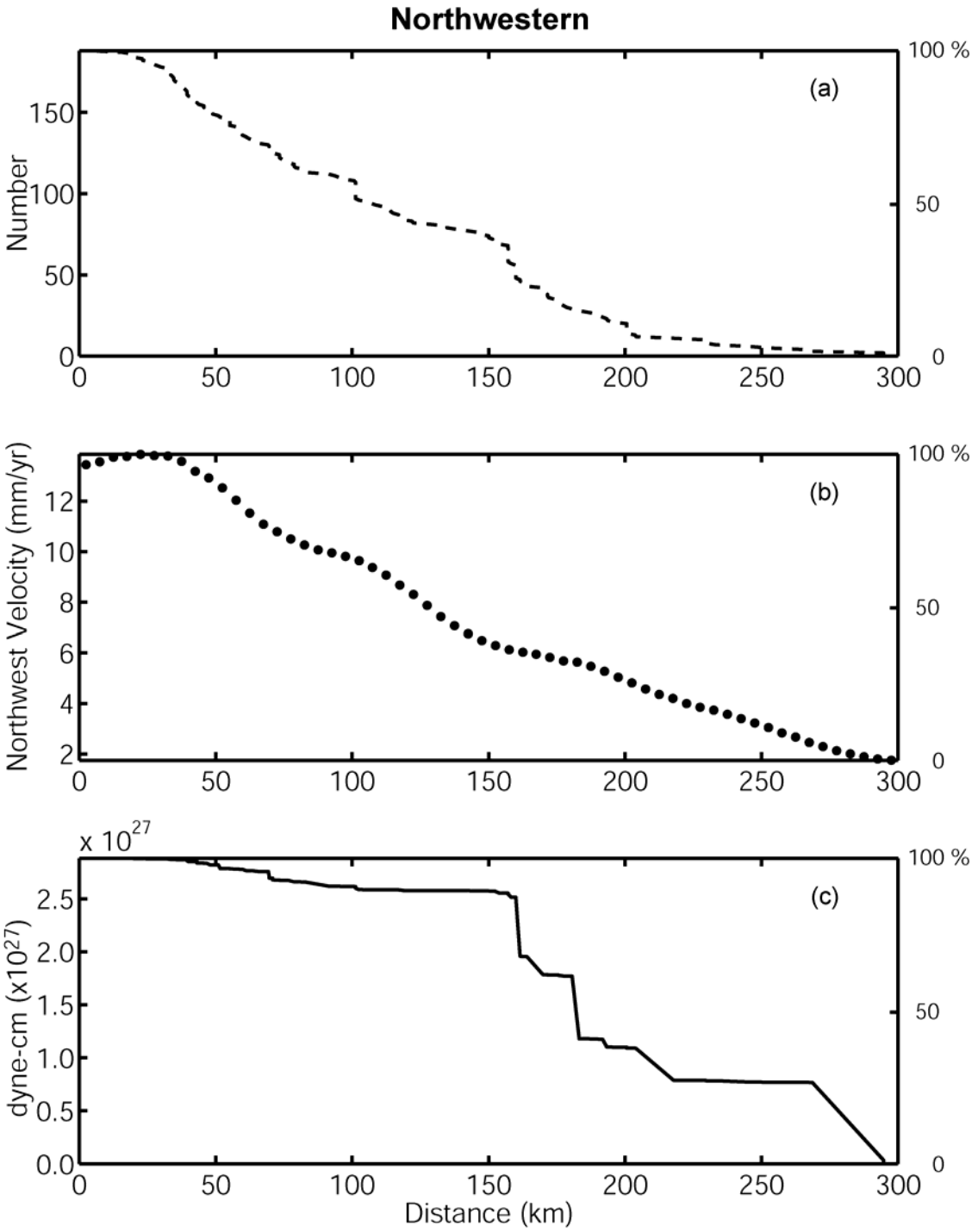


**Figure 2.3** Profiles through three domains, 300 km wide, along the western edge of the province are shown. (a) Cumulative number of earthquake events (b) averaged N37°W components of velocity determined from inversion of geodetic data (Kreemer, personal communication) and (c) cumulative seismic moment release, as a function of the perpendicular distance from the southwestern boundary of the study region (Figure 1).

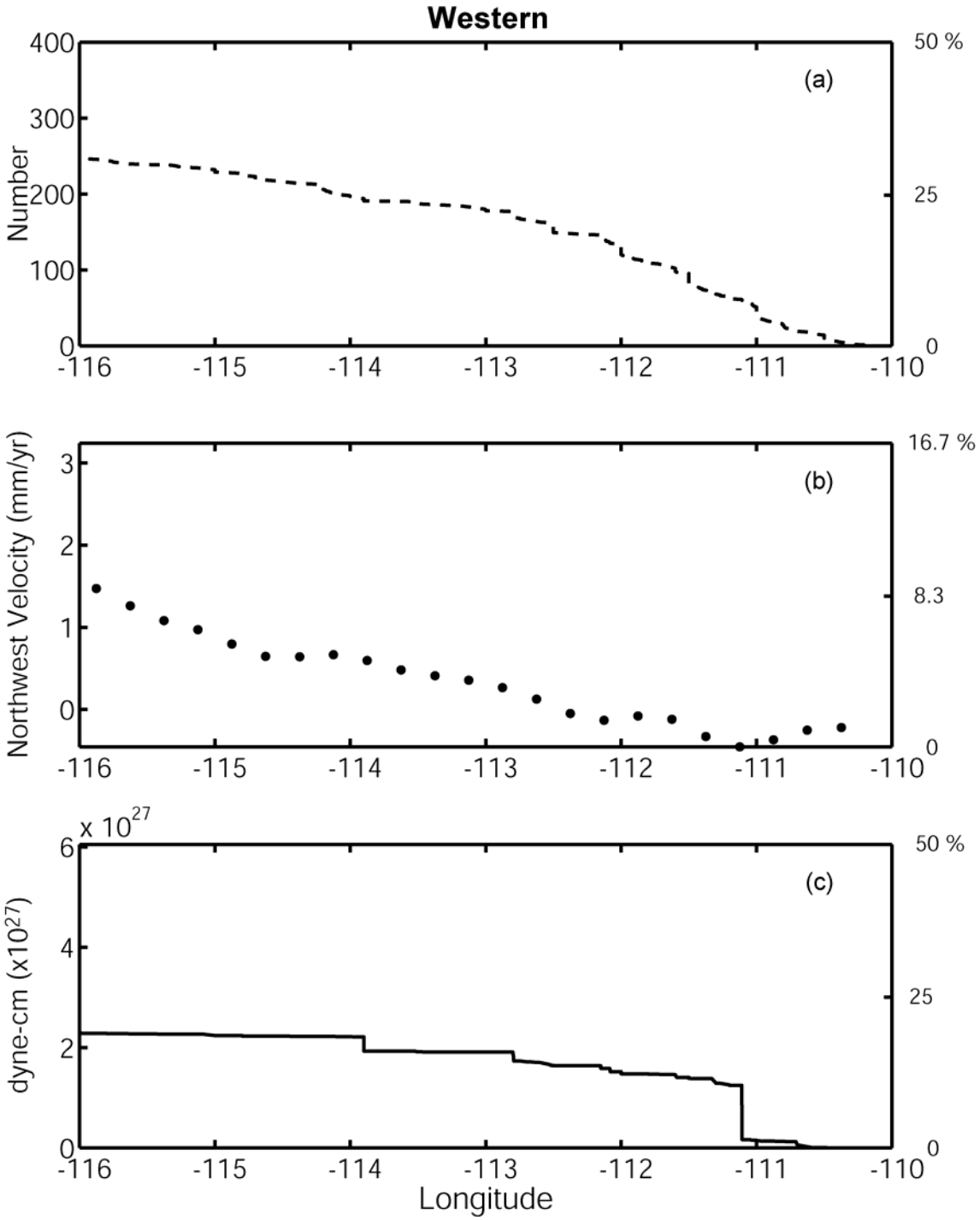


**Figure 2.4** (a) Cumulative number of earthquake events (b) averaged N37°W components of velocity determined from inversion of geodetic data (Kreemer, personal communication) and (c) cumulative seismic moment release, as a function of the east-west distance.

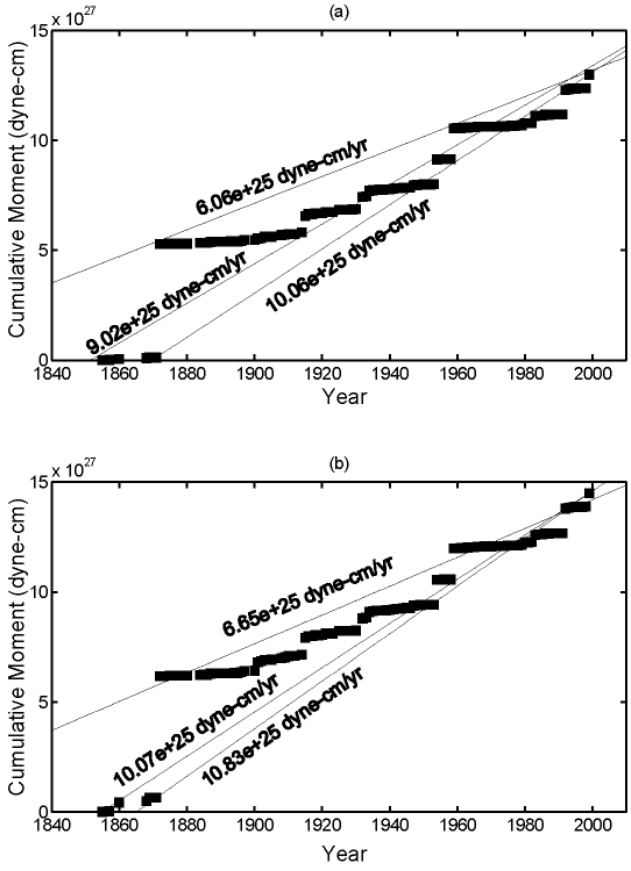


**Figure 3**: (a) Plot of cumulative seismic moment release with time over the study region, based on preferred moment estimates for each earthquake. The lines show the average, and plausible lower and upper bounds, for the seismic moment rate for the region. (b) Same as (a) but based on upper bound moment estimates for the moderate sized earthquakes.

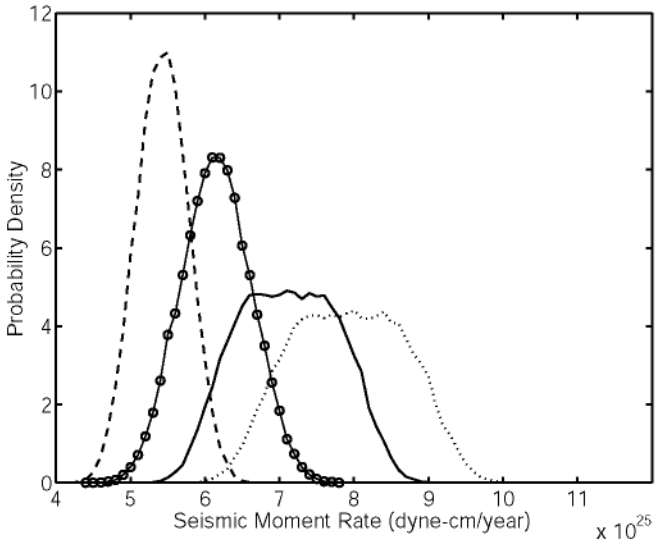


**Figure 4**: Distribution of the average (solid line) and upper (dotted) and lower (dashed) bounds of the seismic moment rates determined from 50,000 Monte Carlo simulations. The distribution due to a least-squares fit to the points is also shown (solid line with circles overlaid). The bin width is 0.1e+25 dyne-cm/yr.

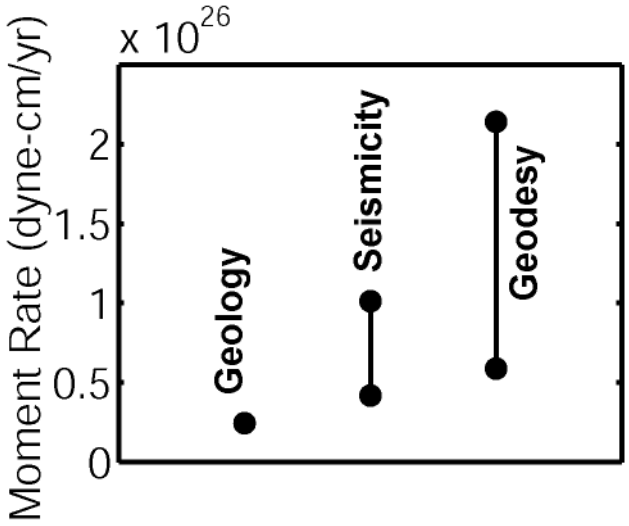


**Figure 5**: Plot showing comparison of the range moment rates determined from the historical seismicity to those determined from geodesy.